Sensors and Actuators B 246 (2017) 477–486

Contents lists available at ScienceDirect

Sensors and Actuators B: Chemical

journal homepage: www.elsevier.com/locate/snb

A highly sensitive, flexible SERS sensor for malachite green detection based on Ag decorated microstructured PDMS substrate fabricated from Taro leaf as template

Pawan Kumar, Robin Khosla, Mahesh Soni, Dinesh Deva, Satinder K. Sharma*

School of Computing and Electrical Engineering SCEE, Indian Institute of Technology (IIT), Mandi, 175001 Himachal Pradesh, India

ARTICLE INFO

Article history:
Received 8 April 2016
Received in revised form 27 January 2017
Accepted 31 January 2017
Available online 14 February 2017

Keywords:
SERS
Flexible
PDMS
Malachite green
Contact angle
Enhancement factor

ABSTRACT

A bio-inspired flexible surface enhanced Raman spectroscopy (SERS) sensor for malachite green (MG) detection has been fabricated by coating Ag on a structured surface of polydimethylsiloxane (PDMS) substrate using textured nano/microstructured Taro leaf as template. The Ag-coated microcavity structured PDMS exhibits high adhesion, hydrophobic behavior (water contact angle $\sim 128 \pm 1^{\circ}$) and serves as a concentrator for the analyte/probe molecule responsible for enhanced SERS intensity. The SERS activity of the fabricated Ag/PDMS flexible sensor having MG as probe molecules shows an enhancement factor of $\sim 2.06 \times 10^5$ over bulk MG molecules. The fabricated SERS sensor is showed the high sensitivity and good signal reproducibility. Sensitivity for very low MG concentration ($\sim 10^{-11}$ M) is reported which is attributed to the presence of high local field produced by Ag granular film and nanovoids onto PDMS surface. AFM and Raman characterizations have revealed the formation of nanovoids on Ag/PDMS structures to create plasmonic hotspots that results in enhanced SERS activity and high sensitivity. Further, the SERS signal under bending strain (tested between 180° and 100° bending), is also detectable for very low concentration of MG (as low as 10^{-7} M) even at substrate bending angles of 100° that establishes the proposed SERS sensor system as an exceptional candidate for flexible MG SERS sensor applications.

1. Introduction

Malachite green (MG) commonly used in textile and paper industries as a dye, antifungal, antiparasitic agent, biocide in seafood, is highly toxic when consumed by human beings. Meanwhile, MG is readily absorbed and metabolizes to the colorless leucomalachite green (LMG) which is mutagenic, genotoxic and carcinogenic in nature that poses serious health risks [1,2]. Due to such harmful effects, the use of MG in consumable aquatic products is either prohibited by law in many countries or the presence of MG is set to a safe level of 1–2 $\mu g\,kg^{-1}$ with in the minimum required performance limit (MRPL) [3,4].

For managing the global health risks and restrictions for use of MG at very low concentration, there is high demand for a sensitive and selective method for the trace detection and monitoring of MG in aquaculture products [3]. In literature, variety of methods for the detection of MG have been reported, such as spectrophotometry [5], high performance liquid chromatography (HPLC) [6,7], liquid chromatography–mass spectrometry (LC–MS) [8], flow injection analysis (FIA) [9], enzyme-linked immune sorbent assay (ELISA) [10], capillary electrophoresis-Raman spectroscopy (CE-RS) [11], surface-enhanced Raman scattering (SERS), etc. [2]. However, most of these techniques are tedious, time-consuming and expensive, due to the involvement of aqueous or organic solvent extractions along with several cleaning up steps including solid phase extractions. A further advantage for SERS-based detection is that the Raman scattering signal is enhanced by several orders of magnitude by the use of metallic nanostructures, where the light-induced phenomena of plasmonic resonance results in intense electromagnetic fields (hot spots). In SERS sensors, the plasmonic nanostructures or the SERS hot spots play an important role for coupling of near field plasmons with vibrational mode of analyte molecules; the coupling results in enhancement of the SERS signal by several orders of magnitude for the analyte molecules [12,13]. The SERS has emerged as a promising method for detection of chemicals and biomolecules due to its molecular level sensitivity and selectivity by giving characteristic Raman signature of the analyte. Owing to such abilities,

* Corresponding author.
E-mail addresses: kmrpwn86@gmail.com (P. Kumar), robin_khosla@students.iitmandi.ac.in (R. Khosla), Mahesh_soni@students.iitmandi.ac.in (M. Soni), d_deva@rediffmail.com (D. Deva), satinder@iitmandi.ac.in (S.K. Sharma).

http://dx.doi.org/10.1016/j.snb.2017.01.202
0925-4005/

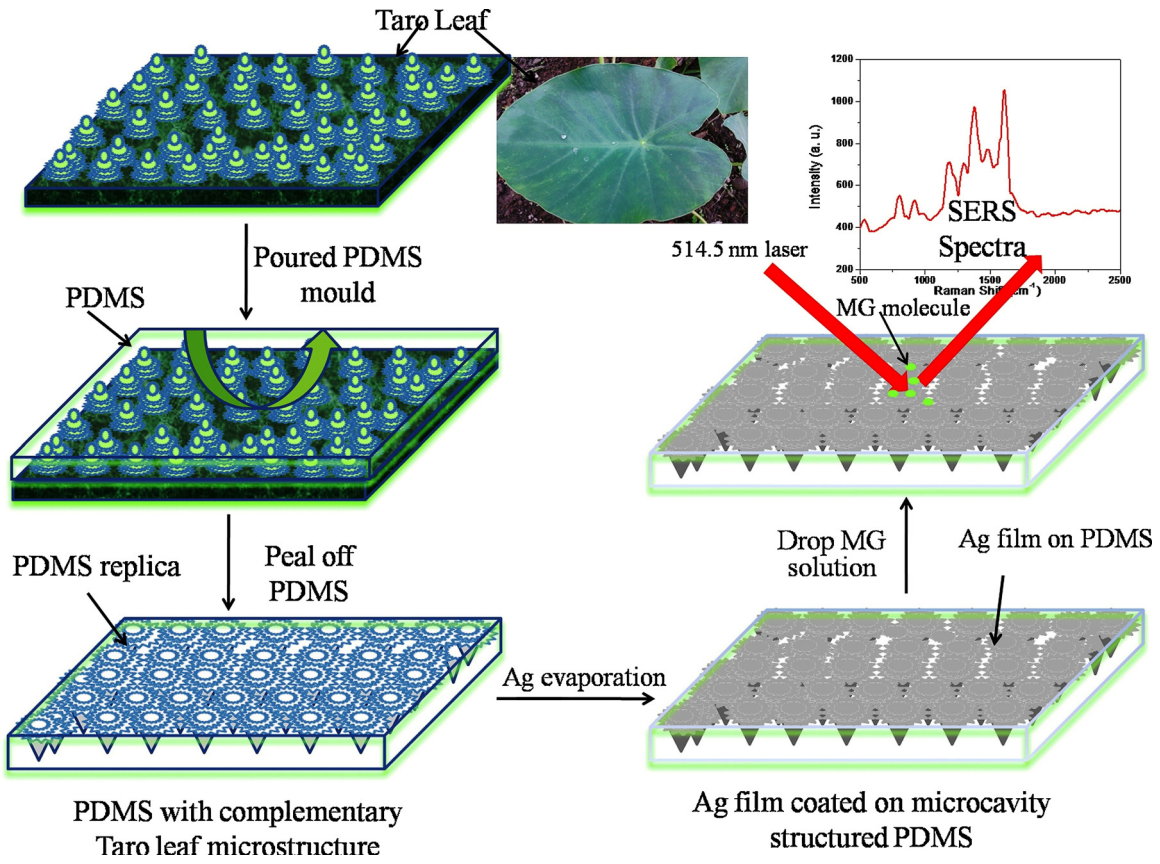

Fig. 1. Schematic for the fabrication of Ag decorated micro-cavity array PDMS SERS substrate using Taro leaf as a template.

SERS has been accepted in a broad range of sensor applications in analytical chemistry, physics, pharmaceuticals, environmental science and in real world applications such as for safety, forensics and terrorist threats [14–17]. However, a major limitation for implementation of SERS sensors for their wider applications is the unavailability of large-area SERS-active substrates with densely decorated periodic and homogeneous nanostructures for obtaining the so-called plasmonic hotspots [13,18]. The cost, complexity of fabrication, reproducibility, and flexibility of substrate for conformal adaptability are other practical considerations to be met for such applications.

In the past, to fabricate the nanostructured SERS active substrates numerous sophisticated techniques have been reported: (i) electron beam lithography (EBL), focused ion-beam lithography (FIB) [19,20], and nanoindentation (NI), etc. approaches offer high precision, control over the shape and size to meet the periodic and homogeneous requirement for nanostructures, though are complex, expensive and have low-throughput. (ii) Soft nanoimprint nanolithography (NIL) [13], conversely is a cost-effective procedure allowing the replication of nanostructures by pressing an elastomeric stamp onto a plastic template surface, but obtaining dense and intense hot spots for SERS within the gaps between metal features is challenging. (iii) Nanosphere Lithography (NSL) [21], Langmuir–Blodgett, etc. [22–25] based self-assembly methods provide high homogeneity but have limited spatial range [26], (iv) Biomimicked structured surfaces to obtain the nano/microstructures on a variety of functional surfaces for SERS sensor applications owing to the unique surface characteristics of certain natural life species. Natural plant leaves such as lotus [27], Taro [28], rice [29], etc., and wings of insects such as of cicada [30], butterfly [31], etc., are known to be comprised of highly homogeneous micro/nanostructures over a large area that are also hydrophobic [32,33]. Whereas, such micro/nano-structures in rose petals [34], peanut leaves [35], and gecko animal's feet [36], show hydrophobicity as well as high adhesion. Various biomimicking studies of SERS sensors have been reported to obtain the desirable homogeneous nanostructures at large scale that are beneficial to obtain high sensor performance. Specifically, due to the intrinsic hydrophobicity and adhesion characteristic of the biomimicked nanostructures of SERS sensor, the probe-analyte concentrate over the nanostructures, results in relatively higher enhancement of SERS sensitivity. Chou et al. [37] have demonstrated such a concentrating effect for probe-analyte on rose petal as SERS substrate having hydrophobicity and adhesion; these properties are also commonly referred in the literature as 'rose-petal effect'. Mo et al. [38] have fabricated bioinspired cicada wings like SERS substrate with switchable adhesion. In other bioinspired SERS sensor studies, Zhang et al. [39] electrochemically fabricated a SERS substrate with micro/nanostructured tetragonal array consisting of Cu and Ag, whereas Tan et al. [40] replicated the 3D sub-micrometer structures of wing scales of butterfly species by photo-reduction process of Ag to generate practical SERS substrates.

Besides above surface structural considerations, the flexibility aspect of SERS sensor has also found attention. Flexibility or bendability offers an easy integration of SERS sensor onto different non-planar shape and size surfaces. Polydimethylsiloxane (PDMS) elastomer that is known to be chemically stable, nontoxic and mechanically flexible in nature besides being inexpensive has been extensively explored for bendable SERS sensor applications [26,41,56].

Furthermore, Kumar et al. [42] fabricated buckled PDMS silver nanorods array as active 3D SERS sensor for detection of bacteria and Singh et al. [43] demonstrated a flexible and disposable strain resistance SERS substrate. For fabrication of large area flexi-

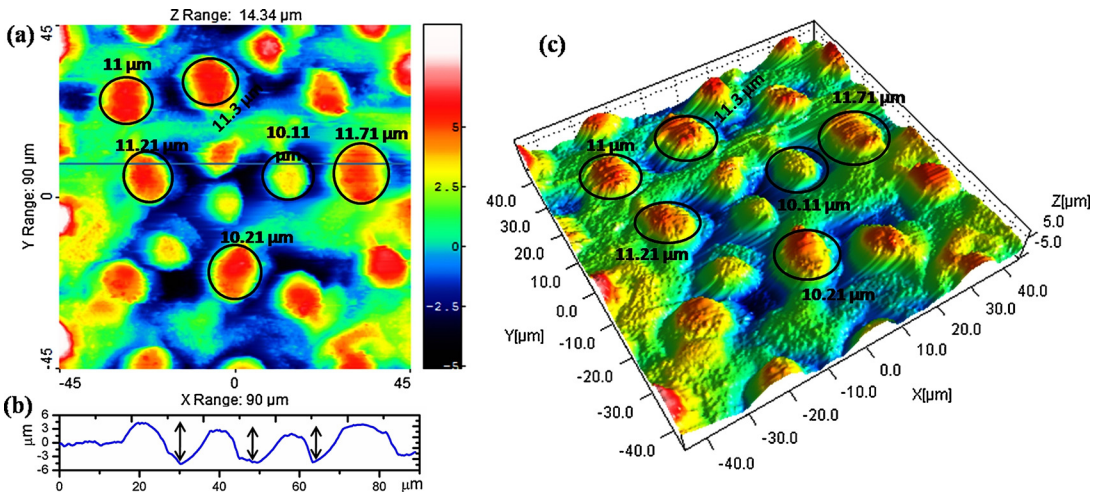

Fig. 2. (a) AFM 2D topography (90 μm × 90 μm) image of Taro leaf surface, (b) the line profile measurement on the AFM image and (c) 3D AFM image (90 μm × 90 μm).

ble PDMS based SERS active substrate, Zhan et al. [44] used transfer printing techniques, while Chung et al. [26] used a shadow mask approach. Similarly, Lee et al. [45] reported flexible filter paper scaffolding as SERS substrates. However, the methods listed in above reports of flexible SERS substrates are expensive, time-consuming due to their multi-step process and are subject to consequences of inconsistent and paradoxical SERS signal.

Given the above status of SERS sensor research, there appears considerable scope for developing a simple, inexpensive but high performance SERS sensor, specifically in the present context for detection of very low concentration of MG. With above objective, in the present work, we choose PDMS as a substrate material for creating desirable and suitable microstructure for SERS sensor and fresh Taro leaf as a template. The Taro plant leaf surface is known to possess a highly homogeneous and hierarchical nano/microscale protrusions or bumps that provide very high water contact angle or hydrophobicity [28]. By casting PDMS mold over the leaf surface a negative pattern of nano/micro scale bumped hierarchical surface structure of Taro leaf is obtained. A homogeneous and hierarchical nano/microcavity natured surface for the PDMS molded SERS sensor is obtained by a simple single step of elastomer molding over a large surface area. Subsequently, for the SERS effect, the Ag metal film has been deposited over the microcavity structured PDMS for obtaining the plasmonic nanostructures (hot spots). Here for the replication, Taro surface microcavities are preferred structure rather than the bumped one. Because, in the literature [49,50] have been reported that the high enhancement factor for the 3D Ag microcavity/nanovoids was due to the coupling of cavity mode with surface plasmon resonance mode. The surface structure characterizations carried out by Atomic Force Microscope (AFM) and Field Emission Scanning Electron Microscope (FESEM) has evidenced that such microcavity/nanovoid structures for the Ag/PDMS SERS sensor applications indeed could be obtained. As described and discussed at the appropriate place in this article, high enhancement factors of the Raman signals for the MG as probe molecule have been obtained. Interestingly, the water contact angle measurements for the prepared Ag/PDMS SERS structure has shown rose-petal effect – the hydrophobicity and adhesion, that may have contributed to enhancement in Raman signal by concentrating MG probe molecules to a small area.

In the present work, the SERS sensor platform fabricated from the above strategy using Taro leaf as template has demonstrated a simple, inexpensive, highly sensitive and flexible PDMS based SERS sensor for detection of very low concentration of MG molecules.

2. Materials and method

2.1. Materials

Elastomer cast for the structured SERS sensor was prepared using commercially available Sylgard-184, PDMS kit, from Dow Corning (USA). Highly pure malachite green dye as SERS probe molecule was purchased from Sigma–Aldrich. The de-ionized (DI) water ~18 MΩ cm^{-1} (Elga PURELAB Classic UV water purification system) was used for dye solution preparation.

2.2. Fabrication method

The Taro leaves collected from cultivated Taro field were dissected into small pieces (5 cm × 5 cm) and fixed with an ultra thin transparent double sided tape in a petri dish (diameter ~60 mm, depth: ~15 mm). The PDMS elastomer was prepared from Sylgard-184 (two-parts, in a weight ratio of 10:1 for parts A and B, respectively) by the addition of part B crosslinking agent to part A in an appropriate ratio. The above elastomer mixture was vigorously hand mixed in a beaker for about 15 min followed by ultrasonication in a water bath for 5 min. The bubbles formed during mixing were removed by desiccating the mixture for 15 min in a vacuum. Thereafter, the PDMS mold was casted on Taro leaf fixed inside the petridish.

The casted PDMS mold in a petri dish was again degassed for 1 h in order to remove air bubbles, particularly at the Taro leaf/transparent tape/petri dish interface, followed by a soft thermal curing at 35 °C for 24 h to ensure the cross-linking of PDMS chains. Thereafter, to prevent the deformation of the PDMS mold surface structure (a negative of Taro leaf) a hard curing was obtained by subjecting a thermal treatment for 2 h at 90 °C. Subsequently, the structured PDMS mold (~2 mm thick) was carefully peeled from the Taro leaf surface as shown in Fig. 1. Further, the structured PDMS molds were cut into ~2 cm × 2 cm dimension as a specimen for surface characterization and for further processing step of Ag metal film deposition. Over one set of the structured PDMS specimen, the Ag thin films (~35 nm) are deposited by thermal evaporator under ultimate pressure of ~5×10^{-6} Torr, using the Ag metal wire of length 1 cm and diameter 1.5 mm.

2.3. Characterization and SERS measurement

The surface topography of the Taro leaf and Ag/PDMS having micro-cavity array on its surface was investigated by atomic force

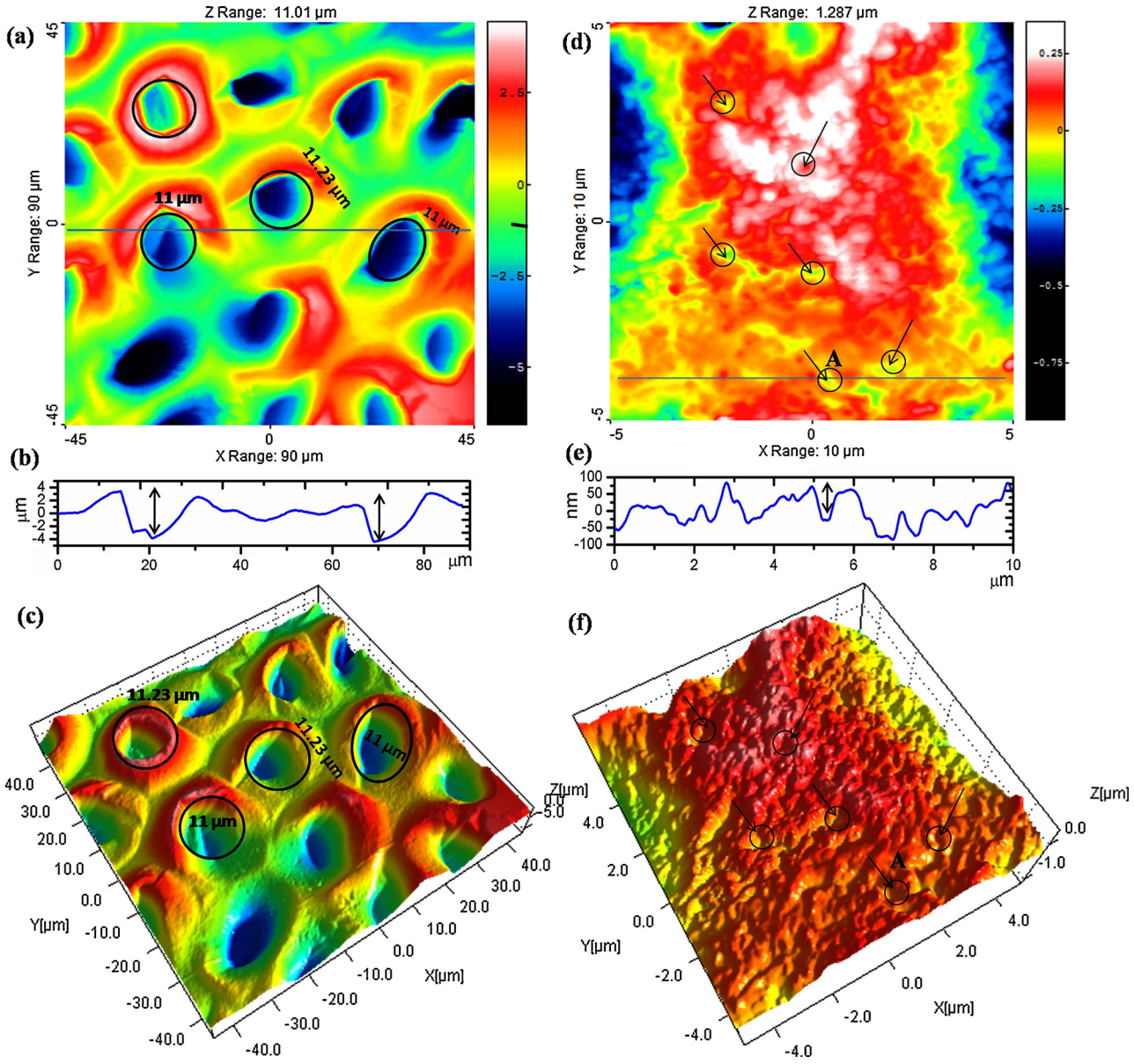

Fig. 3. AFM Images of structured PDMS specimen; (a)–(c) prior to Ag deposition, (d) and (e) post-Ag deposition. (a) 2D (90 μm × 90 μm) image of surface topography of structured PDMS; (b) the line profile measurement on the AFM image in (a); (c) 3D (90 μm × 90 μm) AFM image showing the micro-cavity array of the structured PDMS specimen,; (d) AFM image of 2D (10 μm × 10 μm) topography; (e) line profile measurement on the AFM image in (d); (f) the 3D (10 μm × 10 μm) AFM micrograph of Ag-coated structured Ag/PDMS specimen.

microscopy (AFM; Dimension Icon from Bruker) with a scan rate of 0.5 Hz. The high aspect ratio TESPA-HAR, AFM probe with resonant frequency 320–369 kHz and spring constant k = 20–80 N/m was used for AFM measurement. The contact angle measurements of the DI water on the Taro leaf and structured Ag/PDMS surface were performed with Phoenix 300 system from SEO, Korea. The ~14 μL water droplet was employed to measure the static contact angle. Raman spectra were collected by WiTec CRM-200 confocal Raman system with a 100× objective lens (NA = 0.95) under backscattering configuration. Argon (Ar) ion laser with excitation wavelength (λ = 514.5 nm) was used as the excitation source. The power of the incident laser was maintained at ~6.63 mW on sample throughout the experiments, keeping acquisition time of 60 s for each measurement. MG stock solution of concentration 27 mM had been used for further dilution from 1×10^{-3} to 1×10^{-11} M, using DI water, to serve as molecular probe for the SERS experiments. The MG probe solutions were drop casted on the microstructured Ag/PDMS specimen and dried before SERS measurement.

3. Results and discussion

The AFM topography images (area, 90 μm × 90 μm) of the natural Taro leaf surface for 2D and 3D morphology obtained in tapping mode using tip of high aspect ratio (5:1), are shown in Fig. 2(a) and (c), respectively. These images evidently show that the natural Taro leaf surface consists of an ordered array of microstructure (indicated by circles both in Fig. 2(a) and (c) with bumps or protrusions with average diameter and height of ~11 and ~7.48 μm, respectively). The peak-to-trough dimension of the line profile micrograph in Fig. 2(b) corroborates to the above-observed height of the microstructure bumps. The root mean square (R.M.S.) roughness of Taro leaf surface measured by AFM data (Fig. 2(c)) is ~2367 nm.

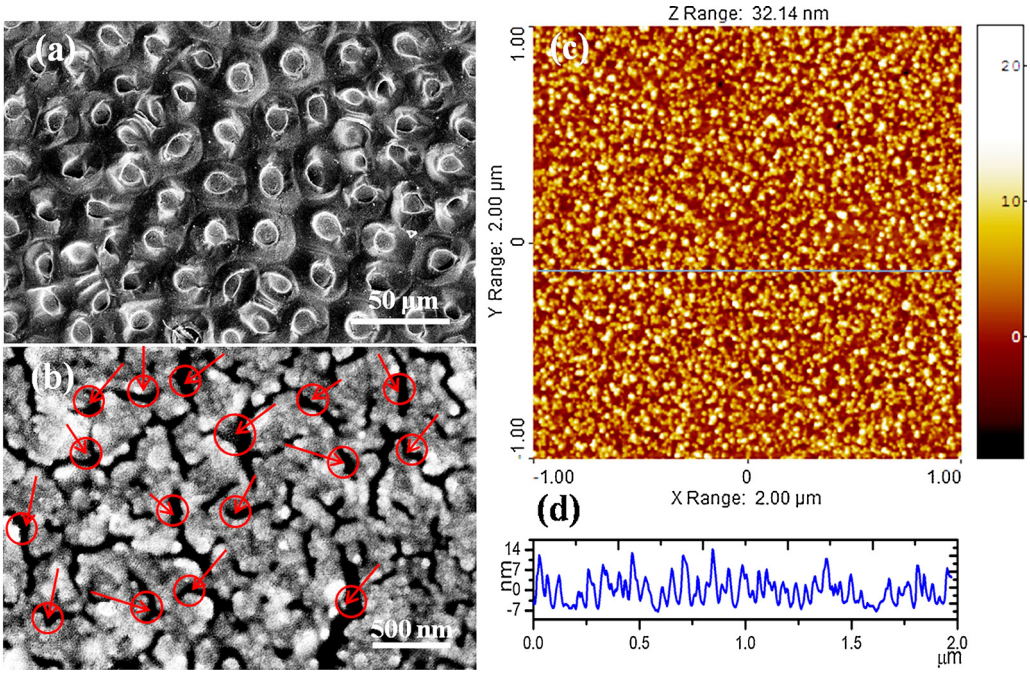

Fig. 4. (a) FESEM image of Ag-coated structured Ag/PDMS specimen (b) a higher magnification FESEM image in (a), (c) AFM image (2 μm × 2 μm) of Ag film deposited on non-structured smooth PDMS surface and (d) is the line profile measurement on the AFM image.

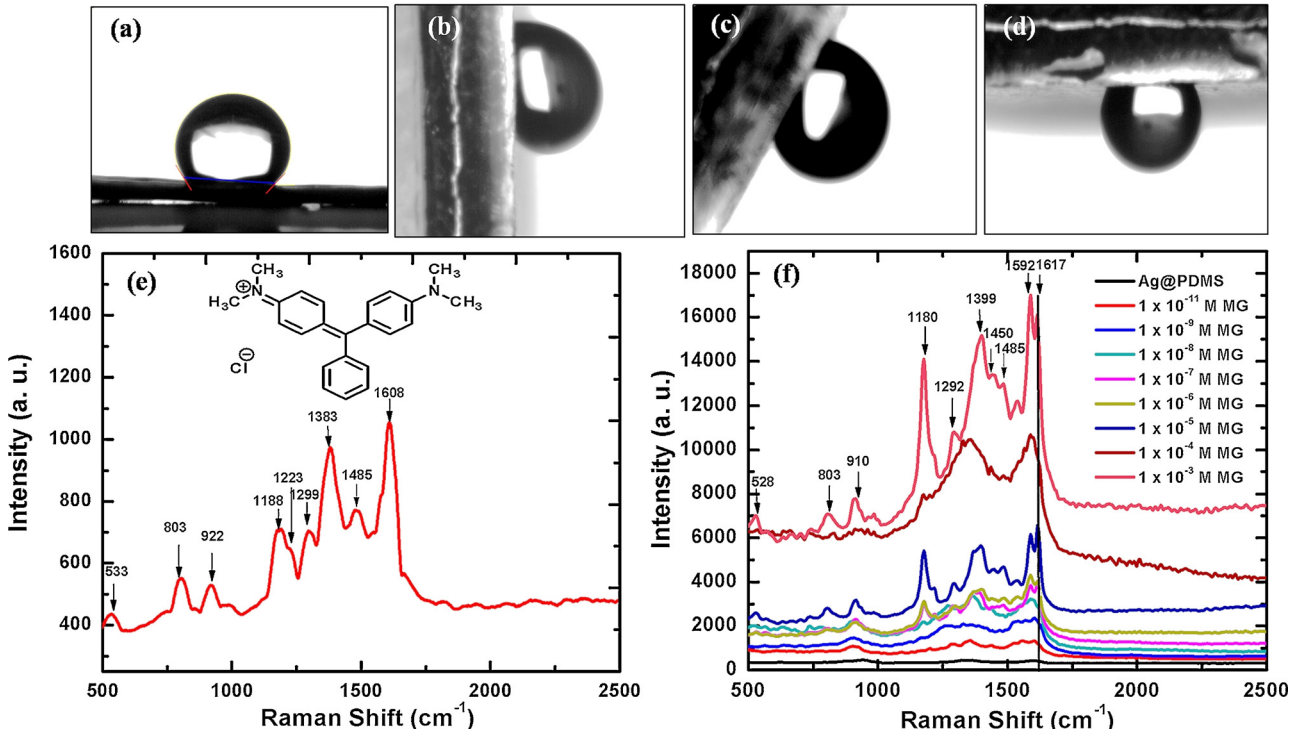

Fig. 5. Contact angle and adhesion measurement at different tilted angle (a) 0°, (b) 90°, (c) 65°, (d) 180° on the surface of microcavity structure Ag/PDMS substrate, (e) Raman spectra of bulk MG on Si substrate as probe molecule with concentration of 27 mM and (f) SERS spectra of MG on Ag/PDMS substrate for various concentration of MG.

As perceive from the AFM micrographs that Taro leaf surface consists of the various micro/nano-scale roughness structures, which offers an potentially opportunity for biomimicking for artificial micro/nano-structures for virous applications.

Results of AFM imaging, performed on the structured PDMS specimen are shown in Fig. 3; Fig. 3(a)–(c) depict surface prior to Ag deposition and Fig. 3(d)–(e) are post-Ag deposition images. The 2D and 3D (90 μm × 90 μm) AFM images in Fig. 3(a) and (c) show an array of uniformly arranged microcavities of dimensions ~11 μm in diameter and ~7.14 μm in depth on PDMS specimen surface. The line profile of these specimen surfaces in Fig. 3(b) corroborates these dimensions for the microcavities. The microcavity nature of structuring on the PDMS is just as expected, being complementary to the bumped structure of the Taro leaf template. These microcavity dimensions match extremely well with Taro leaf bump dimensions measured from AFM images in Fig. 2. The PDMS elas-

Table 1
Assignment for Raman and SERS peaks of MG molecules.

Raman peak position (cm^{-1})	SERS peak position (cm^{-1})	Assignment	Reference
533	528	Phenyl-C-phenyl out-of-plane bending	[47]
803	803	Ring C—H out-of-plane bending ($\gamma(C—H)_{ring}$)	[47,48]
922.8	910	C—H out-of-plane bending, Ring skeletal vibration	[47]
1188	1180	In-plane vibrations of ring C—H ($\delta(C—H)_{ring}$)	[13]
1223	1221	C—H rocking ($\delta(C—H)_{ring}$)	[4]
1299	1292	$\nu(C—C)_{ring}$	[48]
1383	1399	N-phenyl stretching, $\delta(C—H)_{ring}$ and ($\nu(C—C)_{ring}$)	[4]
1485	s-1450, s-1485	$\nu(C—C)_{ring}$ and $\delta(CH_3)$	[47,48]
1608	1592	C—C stretching ($\nu(C—C)_{ring}$)	[47,48]
	1617	Ring C—C stretching ($\nu(C—C)_{ring}$)	[2]

tomer mold envelops the Taro leaf bumps and flows in the recess and reliefs between the bumps resulting to the observed microcavities. This observation is significant and shows the efficacy of the simple PDMS casting method followed in the present work for fabrication of structured SERS sensors.

Fig. 3(d) and (f) show 2D and 3D AFM images for relatively smaller area [10 μm × 10 μm] of Ag deposited structured PDMS specimen. Fig. 3(d) shows that the Ag/PDMS has a nanoscale roughened surface having R.M.S. roughness of ~152 nm. The figure also depicts the presence of nanovoid or nanocavity as marked by the arrows and circles in Fig. 3(f), which affirms this observation. Also, the corresponding line profile of the above AFM images shown in Fig. 3(e) determines the depth of one of the nonvoid as indicated by A (Fig. 3(d)) is found to be ~99 nm. In summary, the AFM images in Fig. 3(a)–(c) for PDMS specimen prior to Ag deposition and in Fig. 3(d) and (e) for the post-Ag deposition demonstrates the presence of microcavities and nanovoids on the surface of fabricated PDMS specimen meant for the SERS sensing being the object for present work.

In order to understand the distribution of microcavity and nanovoid on PDMS specimen surface more clearly, FESEM characterization has been performed. Fig. 4(a) shows the FESEM micrograph of Ag-coated PDMS microcavity array with microcavity diameter size of ~10.4 μm, which is close to the earlier determined dimension by the AFM measurements. A higher magnification FESEM image in Fig. 4(b) reveals the rough surface morphology of Ag/PDMS arising due to the nanogaps (nanovoids) between the metallic coating on the bare structured PDMS surface (as indicated by red arrow and circles) and this again supports the AFM results. Furthermore, the morphology of Ag film deposited on smooth PDMS substrate under similar deposition conditions has been investigated separately by AFM imaging as shown in Fig. 4(c). The AFM (2 μm × 2 μm) scan in the Fig. 4(c) shows that the Ag films are composed of granular Ag nanoparticles, which is further confirmed by the line profile measurement shown in Fig. 4(d).

The wetting property of the Taro leaf and the prepared Ag-coated rough microcavity Ag/PDMS substrate has been investigated by water contact angle measurements. The static contact angle of the fresh Taro leaf and Ag film coated microcavity structure Ag/PDMS substrate is measured as 152 ± 1° (Fig. S1) and 128 ± 1° (Fig. 5(a)) respectively. The contact angle of the Ag/PDMS substrate is less than Taro leaf (Fig. S1), but it is still greater than 90° which shows the microcavity structure Ag/PDMS substrate exhibits hydrophobic behavior.

The adhesion properties of the Ag/PDMS substrate have been studied by tilting the substrate with water droplet at different angles (Fig. 5(a)–(d)). The water droplet is found to stay pinned and not rolling off from the surface when the sample is tilted at different angles 0°, 90°, 65° and 180° as shown in Fig. 5(a)–(d), respectively. Thus, the fabricated Ag decorated Ag/PDMS specimen shows hydrophobicity as well as adhesion or the rose-petal type effect. This phenomenon is interesting and appears to have served well for concentrating analyte molecules on SERS substrate which add to the enhancement of SERS signal as well as in improving the sensitivity for detecting very low concentrations. Although, here, it is interesting to note that the microcavity structure replicated onto PDMS surface are a negative morphology of the bumped hierarchical nano/micro structures of the Taro leaf. Whereas, the Taro leaf is known for its superhydrophobicity due to the water contact angle >150° and the rolling-off or sliding-off the water droplet from the leaf surface at a very small tilt angle of <10° [28]. The present Ag-coated microcavity structures of PDMS as a negative replica of the Taro leaf surface has shown exceptionally higher adhesion, that made the water droplets to completely immobilized.

Fig. 5(e) shows the plots of Raman spectra obtained for MG solution on Si surface at a molar concentration of 27 mM in range of 500–2500 cm^{-1}. All the Raman peaks are matched with MG signature reported in the literature (column1, Table 1).

Furthermore, the bulk SERS spectra for MG ranging from 500 to 2500 cm^{-1} in Fig. 5(f), shows that the various characteristic bands are clearly observed and collerating with the literature. The relatively strong SERS peak at 1617 cm^{-1}, assigned to the in-plane vibrations of ring C—C is still distinguishable for very low concentrations (10^{-9} and 10^{-11} M) of MG. The other peaks of MG at 1399 and 1180 cm^{-1} in the SERS spectrum were caused by N-phenyl stretching and in-plane modes of C—H bending, respectively [46]. The medium bands at 1399, 1221, 910 cm^{-1} are attributed to N-phenyl stretching, C—H rocking, and C—H out-of-plane bending [47]. The assignments for remaining low-intensity Raman peaks at 528, 803, 1292, 1550, 1485 and 1592 cm^{-1} in the MG Raman and SERS spectra are given in Table 1. The SERS spectra, for low MG concentration of 10^{-9} M, is slightly different in shape from the others as shown in Fig. 5(f). This uneven behavior can be explained on the basis of the different orientation of the MG molecules (benzene ring) on the plasmonic substrate, as the orientation of molecules relative plasmonic surface gives rise to slightly distinct SERS signatures [49].

For the quantitative analysis of SERS intensity for various concentrations of MG molecule, the C—C stretching SERS peak at 1617 cm^{-1} in Fig. 5(f) has been chosen to depict the relationship between MG concentration and the observed SERS intensity. As shown in Fig. 6(a), with the concentration of MG molecules from 10^{-11} to 10^{-3} M, the SERS intensity increases monotonously. Significantly, the detection limit for MG, even for a very low 10^{-11} M concentration has been observed, revealing the high sensitivity of fabricated SERS sensor. The high sensitivity of SERS sensor for MG up to 10^{-11} M can be explained by the nanovoids/nanogap formation (Fig. 4(b)) on the surface of Ag/PDMS and granular morphology of the Ag film (Fig. 4(c)), that results in plasmonic hotspots. The formation of these nanoscopic hot spots results in enhancement of the local field (E_{Loc}) and consequently enhance the resultant SERS intensity. Also, the hydrophobic and adhesive behavior of the Ag/PDMS surface, similar to rose-petal effect, further contributes to the enhancement of SERS signal by concentrating the MG molecule over a smaller area during the drying process of MG

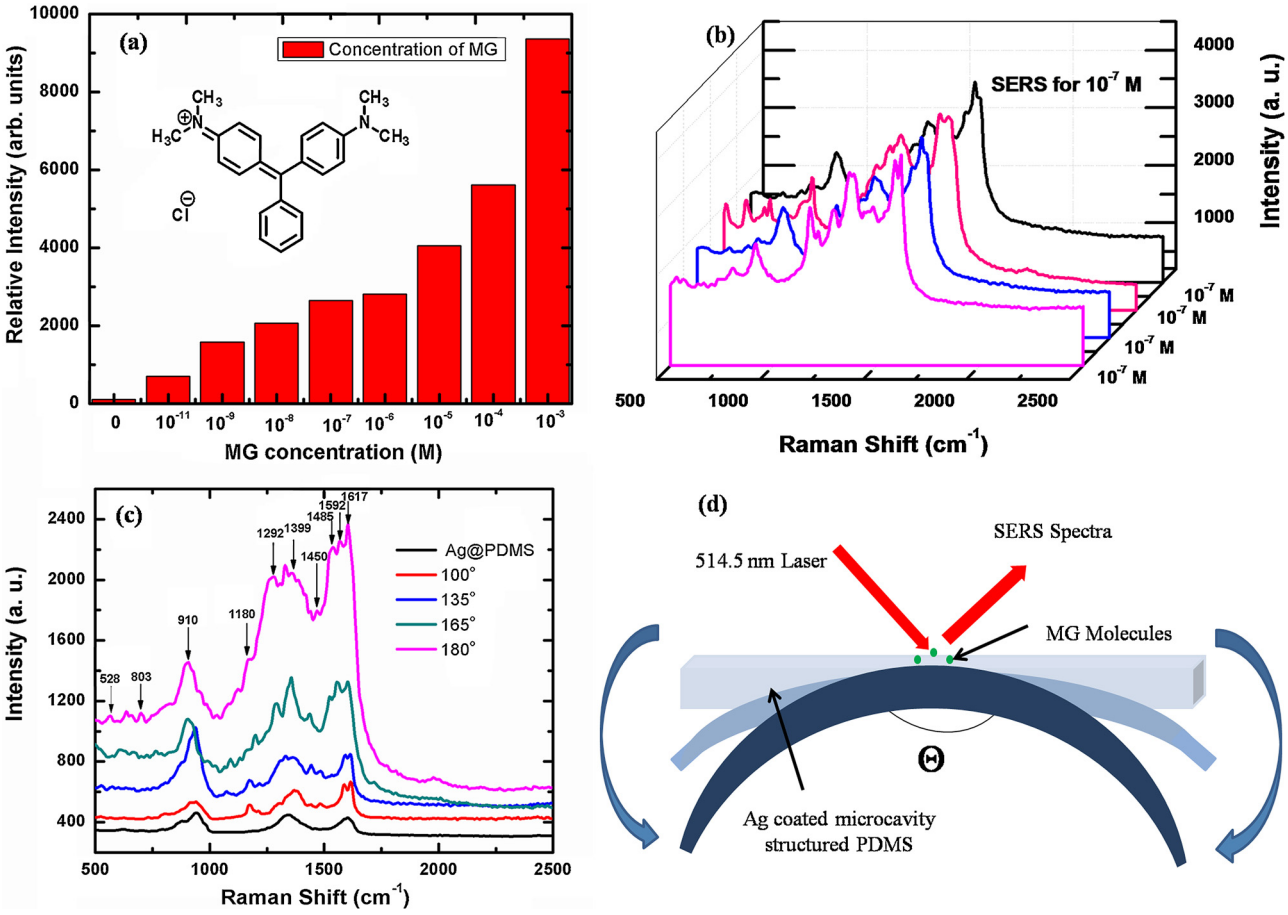

Fig. 6. (a) SERS intensity of Ag/PDMS system for 1617 cm^{-1} peak with variation in MG concentration, and (b) SERS spectra of 10^{-7} M, MG measured at four randomly selected locations on Ag/PDMS substrate, (c) The SERS spectra of the 10^{-7} M, MG concentration with different bending angle (strain) (d) schematic representation of the SERS substrate bending and the measurement of the SERS spectra.

solution [38,50]. This enhanced SERS signal observed in the fabricated Ag/PDMS is due to the concentrating effect. Similar SERS signal enhancement is reported by Chou et al. [37] for rose petal type surface structure having hydrophobic and adhesive properties.

To quantify the extent of the observed SERS enhancements, SERS signal is compared with the Raman signal of the bulk MG. In general, the enhanced intensity for SERS signal compared to normal Raman scattering is due to a very high local electric field (E_{Loc}) in the vicinity of the plasmonic rough surface of SERS substrate. For determining the SERS enhancement effect of Ag/PDMS microcavity array SERS substrate, the SERS enhancement factor (EF) is calculated as follows [51,52]:

$$\mathrm{EF} = \frac{I_{SERS} N_{Bulk}}{I_{Raman} N_{Surface}} \quad (1)$$

where I_{SERS} is the intensity of a vibrational mode in the surface-enhanced spectrum of a given mode, I_{Raman} is the intensity of the same mode in Raman spectrum, N_{Bulk} is the number of bulk molecules probed for a bulk sample, and N_{Surface} is the number of molecules adsorbed on the SERS active substrate.

The Raman spectrum of aqueous MG (1 mM/L) has been used for calculations of enhancement factor. The value of N_{Bulk} and $N_{Surface}$ has been calculated by considering monolayer-absorption mode, assuming the molecules are uniformly distributed in the MG films. The number density of the molecules on films is $(1 \times 10^{-3}\ \mathrm{mol/L} \times 5\ \mu\mathrm{L} \times N_A)/2.5\ \mathrm{mm}^2 = \sim 1.2 \times 10^{15}$, where the surface area of the substrate is 2.5 mm^2, N_A is the Avogadro's number. The laser spot having a diameter of 2 μm has its surface area $\sim 3.14 \times 10^{-6}$ mm^2, hence, the value of $N_{Surface}$ is $(1.2 \times 10^{15} \times 3.14 \times 10^{-6})$, i.e. $\sim 3.7 \times 10^{9}$. During Raman measurements laser spot (of diameter 2 μm) has a depth of 2 μm and considering the size of one MG molecule ~1.3 nm, the number of layers of MG molecules in 2 μM depth is calculated as: $2\ \mu\mathrm{m}/(1.3 \times 10^{-3}) = 1.5 \times 10^{3}$ layers. So, the number of bulk molecules probed in the present measurements for a bulk sample $N_{bulk} = N_{surface} \times$ number of layers $= 3.7 \times 10^{9} \times 1.5 \times 10^{3} \times 27 = 14.9 \times 10^{13}$ (here, the bulk MG solution has 27 mM concentration). The values of I_{Raman} and I_{SERS} are ~593 and ~9366 cm^{-1} respectively, calculated by subtracting the spectrum baseline in origin software. However, for more precise calculations of EF the values of I_{Raman} and I_{SERS} are taken as 205,089.65 and 39,533.7, respectively, calculated by fitting the spectra with multiple Lorentzian functions and finding the area-under-the-curve for the mode at 1617 cm^{-1}. Using Eq. (1), the enhancement factor (EF) calculated for the SERS substrate for 1 mM concentration of MG is $\sim 2.06 \times 10^{5}$. The parameters used for above calculations have been summarized in Table S1.

Additionally, the uniformity and reproducibility of SERS measurements, which are essential parameters for quantitative SERS detection, have been estimated by randomly selecting four different locations on SERS substrate and recording their corresponding SERS spectra for 10^{-7} M concentration of MG. It is observed that for 922 and 1592 cm^{-1} peaks, the measured intensity for four spots on the fabricated SERS substrates shows only a slight variation (4–6%) in intensities, from 900 a.u. (variation, 6%) and from 2500 a.u. (variation,4%), respectively as shown in Fig. 6(b). Since, the SERS spectra

Table 2
Different SERS substrate used for MG detection with their detection range, enhancement factor, and substrate properties.

SERS substrate	Linear detection range	Enhancement factor (EF)	Substrate properties	Reference
Graphene oxide (GO)/Au nanoparticles (NPs) hybrids	2.5–100 μmol/L	3.8×10^3	GO/AuNPs hybrids silicon substrate	[53]
Ag/TiO_2 nanorods scaffold	10^{-7} to 10^{-12} M	4.36×10^5	Non flexible	[13]
Colloidal AuNPs	0.5–35.0 mg L^{-1}(μM)	1.52×10^6	NPs need separation	[4]
Au NWs	10^{-3} to 10^{-6} M	–	Non-flexible	[54]
Starch-coated Ag NPs	0.500–35.0 mg L^{-1} (μM)	5.11×10^5	Powder	[46]
Au nanospheres	1–10 ng g^{-1} (nM)	–	Non-flexible	[47]
Ag/Au NPs coated nanostructured PDMS	2.7×10^{-7} M	3×10^7	Flexible (self assembled PS mono layer)	[44]
Ag NPs on PET	1×10^{-10} M	–	Flexible	[55]
Ag nanoclusters on ZnO nanodome	10^{-5} to 10^{-17} M	$\sim 10^6$	Rigid non-flexible	[13]
Ag/Taro leaf negative PDMS substrate	10^{-3} to 10^{-11}M	$2.06 \times 1\,0^5$	Flexible, hydrophobic,with rose-petal effect	Present study

changes with the orientation of benzene ring [49], as a consequence may contribute to the observed negligible variation (4–6%) in SERS intensity of MG at different locations on the prepared Ag/PDMS SERS substrate.

Table 2 shows comparative results of detection and enhancements for various SERS substrates reported in the literature for MG detection. From Table 2, it is revealed that the fabricated flexible Ag/PDMS SERS substrate for MG detection has higher detection limit (upto 10^{-11} M) as compared to earlier reported flexible SERS substrates. Although, the enhancement factor of certain reported rigid substrates [13] is slightly higher (of order 10^6) than the present Ag/PDMS (2.06×10^5) but they lack the flexibility of SERS substrates precluding their use in flexible applications. Also, a high enhancement factor (3×10^7) reported for the flexible substrate [44] has low spatial surface area due to the used self-assembly based method. In comparison, the presently fabricated flexible Ag-coated PDMS micro-cavity array SERS substrates have shown higher sensitivity as well as high enhancement factor for MG detection due to its concentrating effect (hydrophobic/adhesive, rose-petal effect) and is a large area SERS substrate.

Finally, the effect of substrate bending on SERS intensity (using MG concentration of 10^{-7} M) is investigated by applying bending strain on SERS substrate at different bending angles and recording the corresponding SERS spectra as shown in Fig. 6(c) and (d). Even though, the SERS intensity was found to decrease with the variation in bending angle of substrate from 180° (no bending strain) to 100°, but still the SERS intensity is higher (248 a.u.) compared to the reference value (110 a.u.) and SERS signal for the 10^{-7} M concentration of MG is detectable. The decrease in SERS intensity with bending angle of the substrate from 180° to 100°, is likely due to the increase in nanogap of the nanovoid/cavity on the rough metal surface available on PDMS surface by the application of the bending stress.

4. Conclusion

In summary, a large area flexible ultrasensitive SERS sensor based on Ag-coated structured PDMS substrate for malachite green (MG) detection have been fabricated. The fabrication method includes simple casting of elastomer PDMS on a natural Taro leaf used as a template for creating micro cavity structure over which Ag is deposited by straight forward thin film metal deposition method. The structures on casted PDMS are large area uniform array of micro cavities with diameter ~11 μm and depth ~7 μm. Ag film deposited on the top of the casted PDMS substrate shows a granular nature with nanovoids. The Ag/PDMS surface has shown interesting wetting properties of hydrophobicity (water contact angle $\sim 128 \pm 1°$) as well as exceptionally higher adhesion, signifying a rose-petal effect, which concentrates the probe molecules on SERS substrate and offers high sensing performance. The fabricated SERS sensor showed remarkable high enhancement factor of $\sim 2.06 \times 10^5$ and high sensitivity with a linear range of the detection from 10^{-11} to 10^{-3} M for detection of MG molecules. The reproducibility and uniformity of SERS signal is well within 4–6% variations. The fabricated SERS Ag/PDMS sensor showed the SERS signal in detectable range for the tested MG molecule even on bending (straining) the substrate up to 100° bending strain. The efficacy of the proposed SERS sensors meets several requirements for an inexpensive, simple to fabricate, flexible yet with high enhancement factor as well as high sensitivity and therefore may have the potential for other chemical and biological SERS detection applications.

Acknowledgements

Dr. Satinder K. Sharma is grateful for the financial support from the Department of Science and Technology (DST), New Delhi, India, under a project of the Fast Track (Engineering Sciences) for Young Scientists scheme entitled “Surface Plasmon Based Flexible Colloidal Crystal Sensors, [SERC/ET-0003/2012]”.

Appendix A. Supplementary data

Supplementary data associated with this article can be found, in the online version, at http://dx.doi.org/10.1016/j.snb.2017.01.202.

References

[1] S.L. Stead, H. Ashwin, B.H. Johnston, A. Dallas, S.A. Kazakov, J.A. Tarbin, M. Sharman, J. Kay, B.J. Keely, An RNA-aptamer-based assay for the detection and analysis of malachite greenand leucomalachite green residues in fish tissue, Anal. Chem. 82 (2010) 2652–2660.
[2] Y. Zhang, K. Lai, J. Zhou, X. Wang, B.A. Rasco, Y. Huang, A novel approach to determine leucomalachite green and malachite green in fish fillets with surface-enhanced Raman spectroscopy (SERS) and multivariate analyses, J. Raman Spectrosc. 43 (2012) 1208–1213.
[3] J.X. Dong, C. Xu, H. Wang, Z.-L. Xiao, S.J. Gee, Z.F. Li, F. Wang, W.J. Wu, Y.-D. Shen, J.-Y. Yang, Y.-M. Sun, B.D. Hammock, Enhanced sensitive immunoassay: noncompetitive phage antiimmune complex assay for the determination of malachite green and leucomalachite green, J. Agric. Food Chem. 62 (2014) 8752–8758.
[4] Y. Jin, P. Ma, F. Liang, D. Gao, X. Wang, Determination of malachite green in environmental water using cloud point extraction coupled with surface-enhanced Raman scattering, Anal. Methods 5 (2013) 5609–5614.
[5] I. Safarik, M. Safarikova, Detection of low concentrations of malachite green and crystal violet in water, Water Res. 36 (2002) 196–200.

[6] W.C. Andersen, S.B. Turnipseed, J.E. Roybal, Quantitative and confirmatory analyses of malachite green and leucomalachite green residues in fish and shrimp, J. Agric. Food Chem. 54 (2006) 4517–4523.
[7] G. Chen, S. Miao, HPLC determination and MS confirmation of malachite green, gentian violet, and their leuco metabolite residues in channel catfish muscle, J. Agric. Food Chem. 58 (2010) 7109–7114.
[8] K. Halme, E. Lindfors, K. Peltonen, A confirmatory analysis of malachite green residues in rainbow trout with liquid chromatography–electrospray tandem mass spectrometry, J. Chromatogr. B: Analyt. Technol. Biomed. Life Sci. 845 (2007) 74–79.
[9] T. Sakai, H. Harada, X. Liu, N. Ura, K. Takeyoshi, K. Sugimoto, New phase separator for extraction-spectrophotometric determination of anionic surfactants with malachite green by flow injection analysis, Talanta 45 (1998) 543–548.
[10] M. Yang, J. Fang, T. Kuo, D. Wang, Y. Huang, L. Liu, P. Chen, T. Chang, Production of antibodies for selective detection of malachite green and the related triphenylmethane dyes in fish and fishpond Water, J. Agric. Food Chem. 55 (2007) 8851–8856.
[11] C.H. Tsai, J.D. Lin, C.H. Lin, Optimization of the separation of malachite green in water by capillary electrophoresis Raman spectroscopy (CE-RS) based on the stacking and sweeping modes, Talanta 72 (2007) 368–372.
[12] X. Li, H. Hu, D. Li, Z. Shen, Q. Xiong, S. Li, H.J. Fan, Ordered array of gold semishells on TiO_2 spheres: an ultrasensitive and recyclable SERS substrate, ACS Appl. Mater. Interfaces 4 (2012) 2180–2185.
[13] K. Sivashanmugan, J.D. Liao, B.H. Liu, C.-K. Yao, S.-C. Luo, Ag nanoclusters on ZnO nanodome array as hybrid SERS-active substrate for trace detection of malachite green, Sens. Actuators B 207 (2015) 430–436.
[14] Y. Zhang, K. Lai, J. Zhou, X. Wang, B.A. Rascob, Y. Huang, A novel approach to determine leucomalachitegreen and malachite green in fish fillets with surface-enhanced Raman spectroscopy (SERS) and multivariate analyses, J. Raman Spectrosc. 43 (2012) 1208–1213.
[15] E.Z. Tan, P.G. Yin, T.T. You, H. Wang, L. Guo, Three dimensional design of large-scale TiO_2 nanorods scaffold decorated by silver nanoparticles as SERS sensor for ultrasensitive malachite green detection, ACS Appl. Mater. Interfaces 4 (2012) 3432–3437.
[16] D. Majumdar, A. Singh, P.K. Mondal, S. Kundu, DNA-mediated wirelike clusters of silver nanoparticles: an ultrasensitive SERS substrate, ACS Appl. Mater. Interfaces 5 (2013) 7798–7807.
[17] S.M. Prokes, O.J. Glembocki, R.W. Rendell, M.G. Ancona, Enhanced plasmon coupling in crossed dielectric/metal nanowire composite geometries and applications to surface-enhanced Raman spectroscopy, Appl. Phys. Lett. 90 (2007) 093105.
[18] M.S. Akin, M. Yilmaz, E. Babur, B. Ozdemir, H. Erdogan, U. Tamer, G. Demirel, Large area uniform deposition of silver nanoparticles through bio-inspired polydopamine coating on silicon nanowire arrays for practical SERS applications, J. Mater. Chem. B 2 (2014) 4894–4900.
[19] M. Chirumamilla, A. Toma, A. Gopalakrishnan, G. Das, R.P. Zaccaria, R. Krahne, 3D nanostar dimers with a sub-10-nm gap for single-/few-molecule surface-enhanced Raman scattering, Adv. Mater. 26 (2014) 2353–2358.
[20] H. Xiaoye, M. Guowen, H. Qing, X. Wei, H. Fangming, S. Kexi, Large-scale homogeneously distributed Ag-NPs with sub-10 nm gaps assembled on a two-layered honeycomb-like TiO_2 film as sensitive and reproducible SERS substrates, Nanotechnology 23 (2012) 385705.
[21] A.B. Zrimsek, A.I. Henry, R.P.V. Duyne, Single molecule surface-enhanced Raman spectroscopy without nanogaps, J. Phys. Chem. Lett. 4 (2013) 3206–3210.
[22] N.L. Netzer, Z. Tanaka, B. Chen, C. Jiang, Tailoring the SERS enhancement mechanisms of silver nanowire Langmuir–Blodgett films via galvanic replacement reaction, J. Phys. Chem. C 117 (2013) 16187–16194.
[23] J.C. Hulteen, M.A. Young, R.P. Van Duyne, Surface-enhanced hyper-Raman scattering (SEHRS) on Ag film over nanosphere (FON) electrodes: surface symmetry of centrosymmetric adsorbates, Langmuir 22 (2006) 10354–10364.
[24] Y. Choi, S. Hong, L.P. Lee, Shadow overlap ion-beam lithography for nanoarchitectures, Nano Lett. 9 (2009) 3726–3731.
[25] F.L. Yap, P. Thoniyot, S. Krishnan, S. Krishnamoorthy, Nanoparticle cluster arrays for high-performance SERS through directed self-assembly on flat substrates and on optical fibers, ACS Nano 6 (2012) 2056–2070.
[26] A.J. Chung, Y.S. Huh, D. Erickson, Large area flexible SERS active substrates using engineered nanostructures, Nanoscale 3 (2011) 2903–2908.
[27] A.I. Neto, H.J. Meredith, C.L. Jenkins, J.J. Wilker, J.F. Mano, Combining biomimetic principles from the lotus leaf and mussel adhesive: polystyrene films with superhydrophobic and adhesive layers, RSC Adv. 3 (2013) 9352.
[28] P.P. Peng, Q. Ke, G. Zhou, T. Tang, Fabrication of microcavity-array superhydrophobic surfaces using an improved template method, J. Colloid Interface Sci. 39 (2013) 5326–5328.
[29] G.D. Bixler, B. Bhushan, Rice and butterfly wing effect inspired low drag and antifouling surfaces: a review, Crit. Rev. Solid State Mater. Sci. 40 (2015) 1–37.
[30] M. Sun, G.S. Watson, Y. Zheng, J.A. Watson, A. Liang, Wetting properties on nanostructured surfaces of cicada wings, J. Exp. Biol. 212 (2009) 3148–3155.
[31] S. Nishimoto, B. Bhushan, Bioinspired self-cleaning surfaces with superhydrophobicity, superoleophobicity, and superhydrophilicity, RSC Adv. 3 (2013) 671–690.
[32] K. Liu, X. Yao, L. Jiang, Recent developments in bio-inspired special wettability, Chem. Soc. Rev. 39 (2010) 3240–3255.
[33] Y. Zheng, X. Gao, L. Jiang, Directional adhesion of superhydrophobic butterfly wings, Soft Matter 3 (2007) 178–182.
[34] J. Xi, L. Jiang, Biomimic superhydrophobic surface with high adhesive forces, Ind. Eng. Chem. Res. 47 (2008) 6354–6357.
[35] S. Yang, J. Ju, Y. Qiu, Y. He, X. Wang, S. Dou, K. Liu, L. Jiang, Peanut leaf inspired multifunctional surfaces, Small 10 (2014) 294–299.
[36] K. Autumn, Y.A. Liang, S.T. Hsieh, W. Zesch, W.P. Chan, T.W. Kenny, R. Fearing, R.J. Full, Adhesive force of a single gecko foot-hair, Nature 405 (2000) 681–685.
[37] S.Y. Chou, C.C. Yu, Y.T. Yen, K.T. Lin, H.L. Chen, W.F. Su, Romantic story or Raman scattering? Rose petals as ecofriendly, low-cost substrates for ultrasensitive surface-enhanced Raman scattering, Anal. Chem. 87 (2015) 6017–6024.
[38] X. Mo, Y. Wu, J. Zhang, T. Hang, M. Li, Bioinspired multifunctional Au nanostructures with switchable adhesion, Langmuir 31 (2015) 10850–10858.
[39] Q.X. Zhang, Y.X. Chen, Z. Guo, H.L. Liu, D.P. Wang, X.J. Huang, Bioinspired multifunctional hetero-hierarchical micro/nanostructure tetragonal array with self-cleaning, anticorrosion, and concentrators for the SERS detection, ACS Appl. Mater. Interfaces 5 (2013) 10633–10642.
[40] Y. Tan, X. Zang, J. Gu, D. Liu, S. Zhu, H. Su, C. Feng, Q. Liu, W.M. Lau, W.J. Moon, D. Zhang, Morphological effects on surface-enhanced Raman scattering from silver butterfly wing scales synthesized via photoreduction, Langmuir 27 (2011) 11742–11746.
[41] M.M. Stanton, R.E. Ducker, J.C. MavDonals, C.R. Lambert, W.G. McGimpsey, Superhydrophobic, highly adhesive, polydimethylsiloxane (PDMS) surface, J. Colloid Interface Sci. 367 (2012) 502–508.
[42] S. Kumar, D.K. Lodhi, P. Goel, P. Neeti, J.P. Mishra, Singh, A facile method for fabrication of buckled PDMS silver nanorods arrays as active 3D SERS cages for bacterial sensing, Chem. Commun. 51 (2015) 12411–12414.
[43] J.P. Singh, H.Y. Chu, J. Abell, R.A. Tripp, Y. Zhao, Flexible and mechanical strain resistant large area SERS active substrates, Nanoscale 4 (2012) 3410–3414.
[44] H. Zhan, F. Cheng, Y. Chen, K.W. Wong, J. Mei, D. Hui, W.M. Lau, Y. Liu, Transfer printing for preparing nanostructured PDMS film as flexible SERS active substrate, Compos. B 84 (2016) 222–227.
[45] C.H. Lee, M.E. Hankus, L. Tian, P.M. Pellegrino, S. Singamaneni, Highly sensitive surface enhanced Raman scattering substrates based on filter paper loaded with plasmonic nanostructures, Anal. Chem. 83 (2011) 8953–8958.
[46] Y. Zhao, Y. Tian, P. Ma, A. Yu, H. Zhang, Y. Chen, Determination of melamine and malachite green by surface-enhanced Raman scattering spectroscopy using starch-coated silver nanoparticles as substrates, Anal. Methods 7 (2015) 8116–8122.
[47] Y. Zhang, W. Yu, L. Pei, K. Lai, B.A. Rasco, Y. Huang, Rapid analysis of malachite green and leucomalachite green in fish muscles with surface-enhanced resonance Raman scattering, Food Chem. 169 (2015) 80–84.
[48] Q. Cen, Y. He, M. Xu, J. Wang, Z. Wang, Wavelength dependent resonance Raman band intensity of broadband stimulated Raman spectroscopy of malachite green in ethanol, J. Chem. Phys. 142 (2015) 114201.
[49] S. Schlücker, Surface-enhanced Raman spectroscopy: concepts and chemical applications, Angew. Chem. Int. Ed. 53 (2014) 2–42.
[50] X. Huanga, Y. Zhu, X. Zhang, Z. Bao, D.Y. Lei, W. Yu, J. Dai, Y. Wang, Clam-inspired nanoparticle immobilization method using adhesive tape as microchip substrate, Sens. Actuators B 222 (2016) 106–111.
[51] A.N. Severyukhina, B.V. Parakhonskiy, E.S. Prikhozhdenko, D.A. Gorin, G.B. Sukhorukov, H. Möhwald, A.M. Yashchenok, Nanoplasmonic chitosan nanofibers as effective SERS substrate for detection of small molecules, ACS Appl. Mater. Interfaces 7 (2015) 15466–15473.
[52] D. He, B. Hu, Q.-F. Yao, K. Wang, S.-H. Yu, Large-scale synthesis of flexible free-standing SERS substrates with high sensitivity: electrospun PVA nanofibers embedded with controlled alignment of silver nanoparticles, ACS Nano 3 (2009) 3993–4002.
[53] W.L. Fu, S.J. Zhen, C.Z. Huang, One-pot green synthesis of graphene oxide/gold nanocomposites as SERS substrates for malachite green detection, Analyst 138 (2013) 3075–3081.
[54] A.L. Porta, M. Grzelczak, L.M. Liz-Marzán, Gold nanowire forests for SERS detection, Chem. Open 3 (2014) 146–151.
[55] W. Wu, L. Liu, Z. Dai, J. Liu, S. Yang, L. Zhou, X. Xiao, C. Jiang, V.A.L. Roy, Low-cost, disposable, flexible and highly reproducible screen printed SERS substrates for the detection of various chemicals, Sci. Rep. 5 (2015) 10208.
[56] M. Soni, T. Arora, R. Khosla, P. Kumar, A. Soni, S.K. Sharma, Integration of highly sensitive oxygenated graphene with aluminum micro-interdigitated electrode array based molecular sensor for detection of aqueous fluoride anions, IEEE Sens. J. 16 (2016) 1524.

Biographies

Pawan Kumar was born in Himachal Pradesh, India in 1986. He received the B.Sc. and M.Sc. degree from Himachal Pradesh University, India in 2007 and 2009, respectively. He received the Ph.D. degree in Physics, from the Jaypee University of Information Technology, India in 2015. From 2015 to 2016 he worked as Senior Project Scientist with the school of computing and electrical engineering at Indian Institute of Technology (IIT) – Mandi, Himachal Pradesh, India. He is currently working as a Post-doctoral Researcher at the Research Center for Engineering Science, Graduate School of Engineering and Resource Science, Akita University, Akita, Japan. His research interests include development of high resolution scanning probe microscopy techniques, applications of scanning probe microscopy to dielectric, magnetic thin films, magnetic recording head and investigations of the nano-mechanical and surface properties at the nanometer scale.

Robin Khosla was born in Punjab, India, in 1989. He received the B.Tech. (electronics and communication engineering) and M.Tech. (VLSI Design) degree from Punjab Technical University, Punjab in 2011 and 2013, respectively. He is currently working toward the Ph.D. degree with school of computing and electrical engineering at Indian Institute of Technology (IIT) – Mandi, Himachal Pradesh, India. His research interests include fabrication, characterization and reliability of high-κ dielectrics for CMOS and non-volatile memory applications.

Mahesh Soni was born in Durg, India, in 1988. He received the bachelor's degree in electronics and telecommunication from Chhattisgarh Swami Vivekananda Technical University, Bhilai, India, in 2010, and the master's in VLSI design from NIT Jaipur, in 2012. He is currently pursuing the Ph.D. degree with the Indian Institute of Technology (IIT) Mandi, India. Since 2014, he has been working with S. K. Sharma and A. Soni at IIT Mandi on graphene-based FETs. His research interest includes memory devices and sensors based on graphene and its derivatives for next-generation optimal power high-performance nano-electronic regime devices.

Dinesh Deva was born in Kanpur, India in 1963. He received the M.Sc. degree in Physics from Indian Institute of Technology (IIT) – Roorkee, Uttrakhand, India in 1985. He received the M.Tech. degree in Materials Science from Indian Institute of Technology (IIT) – Kanpur, Uttar Pradesh, India in 1987. He received Ph.D. from CSJM University and Indian Institute of Technology (IIT) – Kanpur, Uttar Pradesh, India in 2008. From 2011 to 2014, he worked as Consultant at the DST Unit on Nanosciences, Department of CHE, Indian Institute of Technology (IIT) – Kanpur, Uttar Pradesh, India. From 2014 to 2016, he worked as consultant for industrial sponsored project at IIT Kanpur. He is currently working as Consultant for the development of Centre for Design and Fabrication of Electronic Devices (C4DFED) at Indian Institute of Technology (IIT) – Mandi, Himachal Pradesh, India.

Satinder Kumar Sharma was born in Himachal Pradesh, India in 1978. He received the M.Sc. degree in Physics (Electronics Science) from Himachal Pradesh University, Shimla (H.P.), India in 2002 and Ph.D. from Department of Electronics Science, on "Silicon based gate dielectric materials for VLSI/ULSI Technology" Kurukshetra University, Kurukshetra-(Haryana), India, in 2007. From 2007 to 2010 he worked as a Post-Doctoral Fellow in DST-Unit on Nanosciences and Nanotechnology, Department of CHE, at Indian Institute of Technology (IIT) – Kanpur, India. He worked as a faculty in Electronics and Microelectronics Division, Indian Institute of Information Technology, (IIIT)-Allahabad, India from 2010 to 2012. He is currently, an Associate Professor, School of Computing and Electrical Engineering (SCEE), Indian Institute of Technology (IIT) – Mandi, (Himachal Pradesh), India. His current research interests include Microelectronics circuits and system, CMOS device, fabrication & characterization, Nano/Micro fabrication & design, polymer nano composite, Sensors, Photovoltaic & self-assembly.